Petroleum Science 20 (2023) 2637–2647

Contents lists available at ScienceDirect

Petroleum Science

journal homepage: www.keaipublishing.com/en/journals/petroleum-science

Original Paper

Organic geochemical and petrographic characteristics of the Cambrian-Ordovician organic-rich marine shales in Scandinavia

Xiao-Wei Zheng [a, *], Niels-H. Schovsbo [b], Lei-Bo Bian [a, c], Arka Rudra [a], Hamed Sanei [a, **]

[a] Lithospheric Organic Carbon (LOC) Group, Department of Geoscience, Aarhus University, 8000, Denmark
[b] Department of Reservoir Geology, Geological Survey of Denmark and Greenland (GEUS), Øster Voldgade 10, Dk-1350, Copenhagen K, Denmark
[c] Research Institute of Petroleum Exploration and Development, PetroChina, Beijing 100083, China

ARTICLE INFO

Article history:
Received 8 July 2022
Received in revised form
28 September 2022
Accepted 13 April 2023
Available online 25 April 2023

Edited by Jie Hao and Teng Zhu

Keywords:
Lower paleozoic
Organic petrology
Initial hydrogen index
Original geochemical properties

ABSTRACT

This work used organic geochemistry and organic petrology to study the depositional environment, organic matter characteristics, and thermal maturity of the Cambrian-Ordovician organic-rich marine shales in the Baltic Basin. The main macerals in Cambrian samples include alginite, bituminite and solid bitumen, while zooclastic macerals become the major proportion of organic matter in the Ordovician samples. As the maturity increase, solid bitumen becomes abundant and dispersed. Semifusinite-like maceral was observed only in Furongian of well DBH15/73, which probably indicates the local intrusion of Permo-Carboniferous dolerite dikes. The programmed pyrolysis results show that immature, early mature, and over-mature samples are developed. However, the data of high-uranium Furongian samples were greatly altered by igneous intrusives from local dikes. HI_o calculation model is simulated based on pyrolysis data and fitted according to the least-square fitting method. The simulated fitting HI_o: 400 mg HC/g TOC (369.5 mg HC/g TOC, 430.5 mg HC/g TOC as 95% confidence bounds) is within the worldwide marine shale HI_o and indicates a marine anoxia and transgressive sea with shallow water column (organofacies B).

1. Introduction

Classification of dispersed kerogen (Type I, II, III, and IV) was based on Van Krevelen's work on coals referring to four 'end-member' compositions of atomic ratios of H/C and O/C. Various kerogen types show distinctly different evolution patterns during maturation (Tissot and Welte, 1984). After the introduction of Rock-Eval pyrolysis (Espitalié et al., 1977), different ranges of the pyrolysis-derived hydrogen index (HI) have been applied for quick kerogen type classification in the petroleum industry (Liu et al., 2022; Pan et al., 2021; Wang et al., 2022; Xu et al., 2022). Kerogen type reveals significant information about the thermogenic petroleum composition, which determines the quality, quantity, and reaction kinetics of petroleum generation (Cai et al., 2022; Ding et al., 2022; Zhu et al., 2022; Hu et al., 2018, 2021). However, there is no discrete and uniform organic matter composition in kerogen, hence different organic constituents have distinct physiochemical evolution pathways during maturation.

The lower Paleozoic shales have atypical hydrocarbon generation characteristics from the common marine kerogen types (Horsfield et al., 1992; Zheng et al., 2022). Their organic matter composition and thermal maturity evolution have aroused great attention as the lower Paleozoic shales are important source rocks and unconventional hydrocarbon plays globally (Luo et al., 2020). Previous works about the lower Paleozoic shales indicated various kerogen types, ranging from type II to type III (Sanei et al., 2014). These shales have relatively low hydrogen index (HI), high degree of aromaticity, and gas-prone characteristics (Horsfield et al., 1992; Sanei et al., 2014), which is atypical for the organic geochemistry of marine type kerogen. The possible explanations could be uranium related alteration (Yang et al., 2018; Zheng et al., 2021a), unusual chemistry of the biota precursor (Sanei et al., 2014), or the contribution of abundant graptolite to the dispersed organic matter (Luo et al., 2017).

A systematical report of the source rock would be of significant reference value to hydrocarbon resource assessment of the lower Paleozoic rocks. In this work, organic geochemistry and petrography

* Corresponding author.
** Corresponding author.
E-mail addresses: zhengxiaowei1103@outlook.com (X.-W. Zheng), sanei@geo.au.dk (H. Sanei).

https://doi.org/10.1016/j.petsci.2023.04.011

are applied to determine the organic matter composition of the Cambrian-Ordovician shales in the Baltic Basin. To understand the evolution of the source rock and to provide an effective evaluation of the hydrocarbon generation capacity, a complete organic matter evolution model along with the maturation process is established.

2. Sample and methods

The Alum Shale Formation (Nielsen and Schovsbo, 2006) comprised a middle Cambrian (Miaolingian) to the Lower Ordovician (Tremadocian) marine succession deposited with an overall transgression of the palaeocontinent Baltica (Fig. 1, Thorslund, 1968; Nielsen and Schovsbo, 2006; Schovsbo et al., 2016). Previous tectonic evolution research, which focused on southernmost Sweden, Bornholm, and the Baltic Sea region, proposed that this area is hosted on a large-scale releasing bend in the dextral strike-slip system with its resulting pull-apart basins (Erlström et al., 1997). High paleo-productivity and well-anoxic condition resulted in the deposition of black to dark brown organic-rich shale combined with subordinate fossiliferous bituminous limestone. It exhibits a remarkable uniform lithology (Schulz et al., 2021), and the organic matter is of algal, bacterial and fauna origin (Petersen et al., 2013; Sanei et al., 2014). High-resolution biostratigraphy of Cambrian trilobite and Ordovician graptolite enables detailed

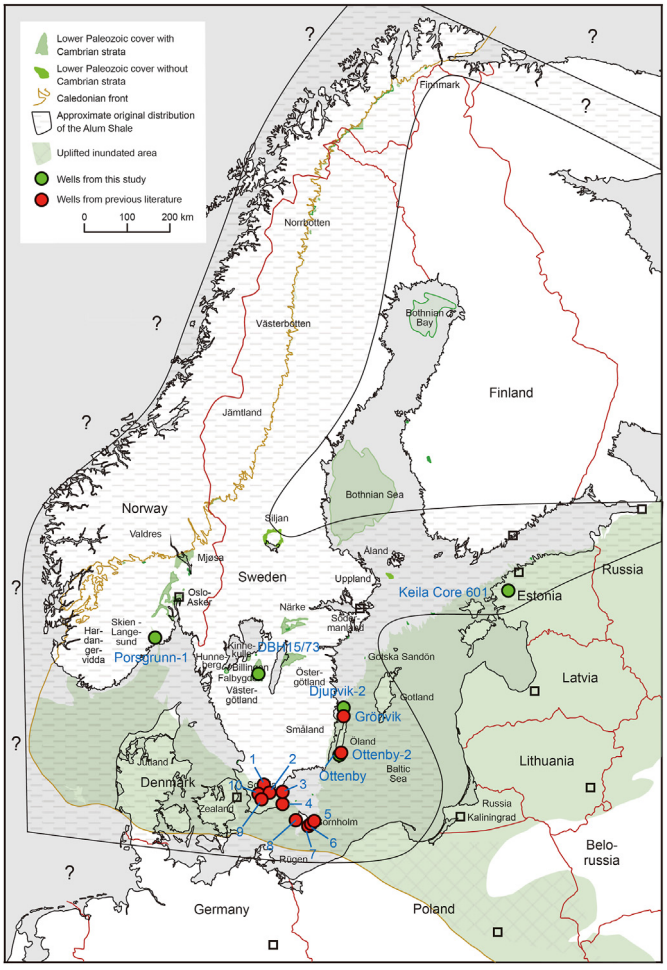

Fig. 1. Geological setting and locations of studied Baltic samples (Modified from Schovsbo et al., 2018). 1-Klinta, 2-Bjärsjölagård, 3-Kivik, 4-Gislövhammar, 5-Øleå at Borggård, 6-Øleå at Billegrav, 7-Øleå at Slusegård, 8-Læså at Vasagård, 9-S.Sandby, 10-Röverakulan, 11-Ottenby, 12-Grönvik.

stratigraphic correlation (Fig. 2). Different regional subsidence and uplift, as well as metamorphism by igneous intrusives (Permo-Carboniferous), led to a wide range of maturity (Schulz, 2021). In this work, 187 core samples collected from 6 wells and outcrops are widely distributed in the Baltic basin (Fig. 1, Table 1).

Bulk pyrolysis geochemistry of the Baltic samples has been conducted using the HAWK pyrolysis and TOC analyser (Wildcat Technologies) in the Lithospheric Organic Carbon (LOC) lab, Department of Geoscience, Aarhus University, Denmark (Zheng et al., 2021a). Organic parameters such as total organic carbon (TOC, wt.%), S1 (mg HC/g), S2 (mg HC/g), hydrogen index (HI, mg HC/g TOC), oxygen index (OI, mg CO_2/g TOC), T_{max} (°C) are reported in this paper.

Organic petrology is an effective supplemental method to provide organic matter assemblage and grade of the evolution of finely disseminated kerogens visually (Pang et al., 2022). The identification of organic matter constituent was conducted using reflected white light and fluorescence-inducing UV light Zeiss Axio Image II microscope, equipped with Discus-Fossil system (Hilgers, Konigswinter, Germany) at LOC lab, Aarhus University. Samples were sieved to 63 μm to 1 mm rock chips and embedded in epoxy with random orientation, then grounded and polished to obtain a measurable surface suitable for oil immersion. The system was calibrated against a standard of R_o: 1.317% (N-LASF). Due to the absence of vitrinites in the pre-Devonian rocks, the reflectance measurements were carried out on solid bitumen and graptolite under oil immersion (objective × 50). All the reflectance values were transferred into VR_{oeqv} (%) according to $VR_{oeqv} = 0.73 \times R_{o(graptolite\ +vitrinite\text{-}like)} + 0.16$ (Petersen et al., 2013) for graptolite and $VR_{oeqv} = 0.618 \times BR_o + 0.4$ (Jacob, 1989) for solid bitumen, to provide the data of organic matter maturity.

Uranium concentration was determined using Inductively Coupled Plasma Mass Spectrometry (ICP-MS) at Acme Laboratory in Vancouver, Canada. Detailed experimental procedures could be found in Zheng et al. (2021a).

3. Results

3.1. Organic petrology

The microscopically identifiable organic components in the Baltic lower Paleozoic shales include alginite, liptoderinite, bituminite, solid bitumen, vitrinite-like, graptolite fragments, and semifusinite-like. Semifusinite belongs to the inertinite maceral group, which shows intermediate reflectance and preserved plant cell structures (leaf-, or wood-derived) characterized by parenchymatous and xylem tissues of stems. Semifusinite frequently shows irregular anisotropy and the reflectance of semifusinite increases as the degree of dehydration and oxidation of its precursors' increase (ICCP, 2001). However, the herbaceous plants and leaves (composed of cellulose and lignin) are not developed in pre-Devonian rocks, therefore, we classify this maceral as semifusinite-like, which are only discovered in the Furongian samples in well DBH15/73 (Fig. 3a, 3b). Liptinite is dark grey to black in reflected white light and has yellow to orange fluorescence under UV light (Fig. 4a, 4b, 4d). Structural alginite is mainly present as lamalginite and telaginite, while liptoderinite is of small particle size and may consist of fragments or relicts of the other liptinite macerals (Fig. 4a, 4d). The most abundant recognizable fluorescing organic matter is structural alginite in immature samples (e.g., Djupvik-2, Core601), however, amorphous organic matter (bituminite) and fluorescent organic-clay mixture become more abundant in the early mature shales (e.g., Ottenby-2 and Hällekis-1, Fig. 4b, 4c, 4d). Bituminite is characterized by lacking a definite shape and is developed in perpendicular sections or as a more

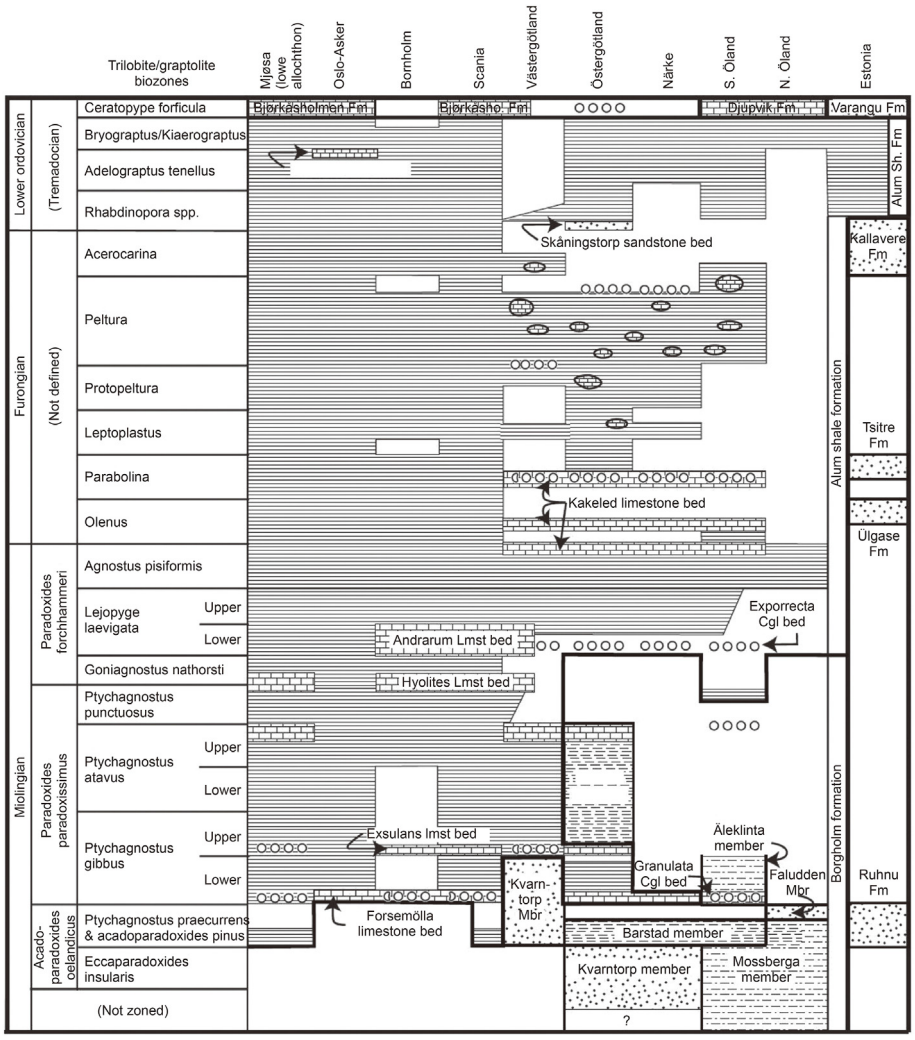

Fig. 2. Lithostratigraphy of the Alum shale and coeval strata in Scandinavia and northern Estonia (after Nielsen and Schovsbo, 2006, Schovsbo et al., 2018, Nielsen et al., 2020).

Table 1
Sample location, depth, formation and sample amount (N).

Outcrop/Well Name	Formation	Location	Depth, m	N
Djupvik-2	Tremadoc	N. Öland, Sweden	5.5–2.2	13
Core601	Tremadoc	Keila, Estonia	47.9–43.2	15
Hällekis-1	Furongian	Västergötland, Sweden	23.4–34.1	10
Ottenby-2	Miaolingian-Tremadoc	S.Öland, Sweden	29.7–1.6	50
DBH15/73	Miaolingian-Furongian	Västergötland, Sweden	153.8–128.9	77
Porsgrunn	Miaolingian-Furongian	Porsgrunn, Norway	309.9–264	22
Röverakulan	Up.Silurian: Ludlow	Scania, Sweden	Outcrop	1
Klinta	Up.Silurian: Ludlow	Scania, Sweden	Outcrop	1
Bjärsjölagård	Up.Silurian: Ludlow	Scania, Sweden	Outcrop	1
Øleå at Slusegård	Low.Silurian: Wenlock	Bornholm, Denmark	Outcrop	1
Øleå at Billegrav	Low.Silurian: Llandovery	Bornholm, Denmark	Outcrop	1
Læså at Vasagård	Up.Ordov	Bornholm, Denmark	Outcrop	1
Kivik	Mid.Ordov	Scania, Sweden	Outcrop	1
Ottenby	Tremadoc	Öland, Sweden	Outcrop	1
Gislövhammar	Tremadoc	Scania, Sweden	Outcrop	1
S.Sandby	Furongian	Scania, Sweden	Outcrop	1
Grönvik	Miaolingian	Öland, Sweden	Outcrop	1
Øleå at Borggård	Miaolingian	Bornholm, Denmark	Outcrop	1

homogeneous, diffused, equidimensional particles in various shapes in horizontal sections (Pickel et al., 2017; Hackley et al., 2018). Since bituminite is a product of variable organic matter undergoing alteration or degradation at different levels, its fluorescence varies widely (Fig. 4b, 4c, Pickel et al., 2017). The fluorescent organic-clay mixture usually shows yellow to brown

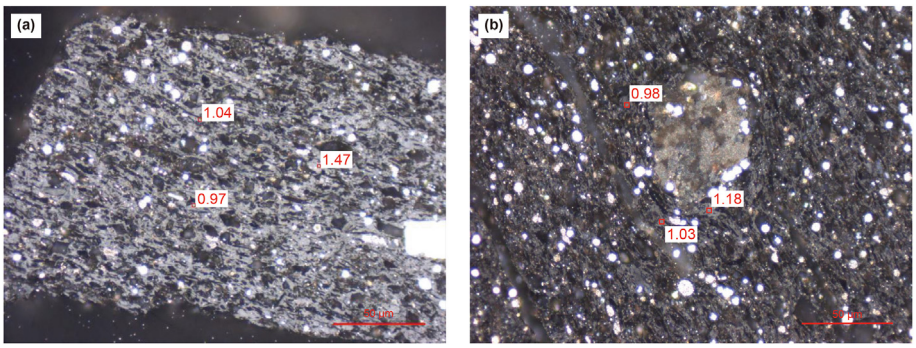

Fig. 3. Photomicrographs of semi-fusinite in Alum shale: (a) sample DBH5069 (upper Cambrian); (b) 'contemporaneous deformation structure' of the semi-fusinite in sample DBH5069.

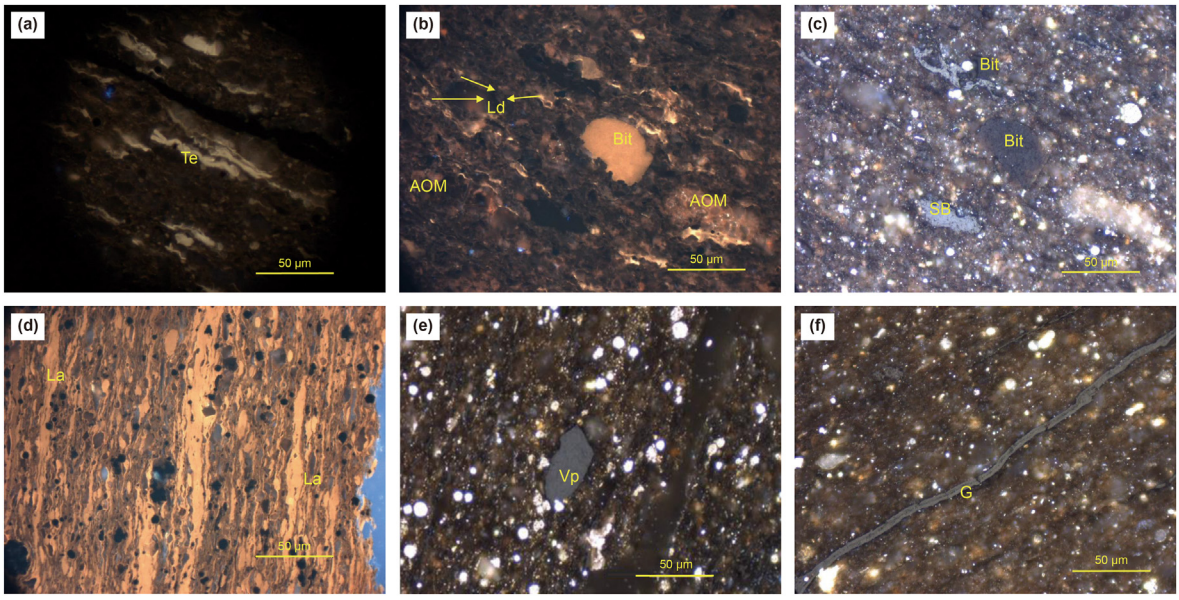

Fig. 4. Photomicrographs of macerals in the Alum shale: (a) Sample Dju2014; (b) Sample Ott1027 in Fluorescence light; (c) Sample Ott1027 in white light; (d) Sample 21423 from Hällekis-1; (e) Sample DBH5140; (f) Sample EST3008. Abbreviation: Te: telaginite; Ld: liptoderintie; AOM: fluorescing amorphous organic matter; Bit: bituminite; SB: solid bitumen; La: lamalginite; Vp: vitrinite-like particle; G: graptolite.

background fluorescence, as lipid substances interlayered or adsorbed with clay minerals (Fig. 4d). Vitrinite-like maceral are organic fragments, which resemble physical and petrographic similarities to vitrinite, characterized by a smooth polished surface that reflectance can be measured on (Fig. 4e). Vitrinite-like macerals are widely discovered in the lower Paleozoic sediments globally (Buchardt and Lewan, 1990; Xiao et al., 2000; Petersen et al., 2013), however, the origin or precursor of this maceral is still unclear. Graptolite can be divided into non-granular and granular, often characterized by fusellar layers and growth nodes (Fig. 4f). Graptolite fragments are the predominant maceral in Ordovician samples (Zheng et al., 2022, Fig. 4f).

The solid bitumen observed in this work is classified as diagenetic solid bitumen, initial-oil solid bitumen, primary-oil solid bitumen, and pyrobitumen, according to Sanei's classification (Sanei, 2020). Diagenetic solid bitumen is an amorphous solid to semi-solid organic groundmass in dark grey color and is often malleably deformed by compaction (Fig. 5a, Sanei, 2020). Diagenetic solid bitumen is not a secondary maceral from kerogen thermal cracking. It originates from biodegradation and low-temperature alteration of bituminite or AOM in the immature stage (Sanei, 2020). Initial-oil solid bitumen is amorphous, grey color, often non-fluorescing organic matter (Fig. 5b). It is referred to as a precursor of crude oil and derived from cracking of oil-prone organic matter and generated as heavy, viscous bitumen. Primary-oil solid bitumen has a flow and void filling structure (Fig. 5b), suggesting it is derived from the migration of liquid petroleum. The dispersed and distribution pattern of these bitumen networks suggested the oil generation stage, but could also be influenced by the viscosity and pore network size and quality (Sanei, 2020). Pyrobitumen is a non-generative form of solid bitumen with high reflectance (Fig. 5c). It is derived from the intense thermal alteration of previously generated solid bitumens. Pyrobitumen is widely identified in overmature samples, e.g., Porsgrunn samples. Solid bitumen in immature and early mature samples are mostly diagenetic solid bitumen, while the proportion of post-oil solid bitumen with higher reflectance, and different connecting and dispersed level increase as the sample maturity increase.

VR_{oeqv} data are summarized in Table 2. Alum shale samples have differing maturity levels, containing immature to early mature (VR_{oeqv} of sample Grönvik is 0.39%. VR_{oeqv} range of 0.53–0.66% in

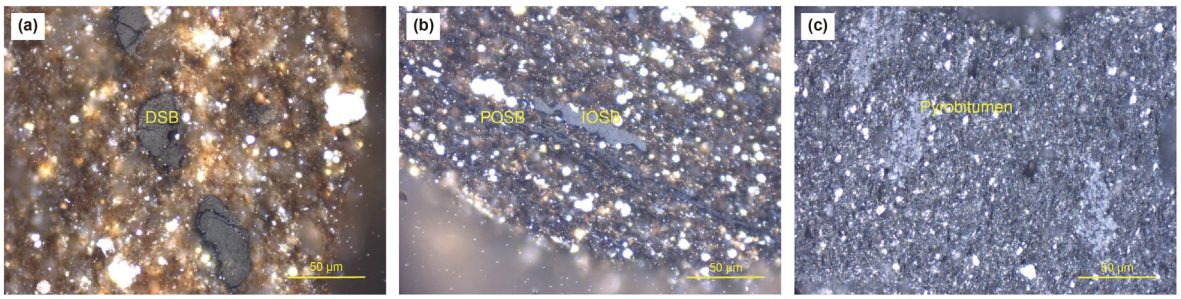

Fig. 5. Photomicrographs of solid bitumen in the Alum shale: (a) Sample Dju2008; (b) Sample DBH5018; (c) Sample Por4002. Abbreviation: DSB: diagenetic solid bitumen; IOSB: initial-oil solid bitumen; POSB: primary-oil solid bitumen.

Table 2
Mean and data range of TOC, T_{max} and VR_{oeqv}.
Since T_{max} is not useful in over-mature samples since invalid S2 signal in highly mature source rock, T_{max} values given in samples with low S2 values were regarded as not representative.

Well Name	TOC			T_{max}			VR_{oeqv}		
	Range	Mean	N	Range	Mean	N	Range	Mean	N
Djupvik-2	1.6–12	8	13	417–429	422	21	0.53–0.66	0.6	4
Core601	3.1–11.6	9.5	15	410–417	413	15	0.53–0.61	0.59	5
Hällekis-1	8.9–28	16	10	412–421	417	10	0.49–0.56	0.53	2
Ottenby-2	0.4–13	7	50	388–437	425	79	0.61–0.74	0.68	6
DBH15/73	0.3–15.8	6	77	394–440	420	144	0.53–1.39	0.93	8
Porsgrunn	0.2–1.9	1.1	22	/	/	22	2.1–2.5	2.3	2
Röverakulan	0.33		1	456			0.83		1
Klinta	0.36		1	430			0.98		1
Bjärsjölagård	0.43		1	434			0.71		1
Øleå atSlusegård	0.93		1	/			1.95		1
Øleå at Billegrav	1.26		1	596			1.77		1
Læså atVasagård	2.04		1	595			1.92		1
Kivik	1.22		1	512			1.51		1
Ottenby	8.01		1	437			0.71		1
Gislövhammar	8.42		1	475			1.42		1
S.Sandby	7.14		1	596			1.66		1
Grönvik	8.79		1	418			0.39		1
Øleå at Borggård	5.59		1	/			1.70		1

Djupvik-2, 0.53–0.61% in Core601, 0.49–0.56% in Hällekis-1, and 0.61–0.74% in Ottenby-2), mature (Outcrop sample Röverakulan, Klinta, Bjärsjölagård and Ottenby have VR_{oeqv} at 0.83%, 0.98%, 0.71% and 0.71% respectively), and overmature (VR_{oeqv} of Øleå at Slusegård, Øleå at Billegrav, Læså at Vasagård, Kivik, Gislövhammar, S.Sandby and Øleå at Borggård are 1.95%, 1.77%, 1.92%, 1.51%, 1.42%, 1.66% and 1.70% respectively. VR_{oeqv} range of 2.1–2.5% in Porsgrunn). DBH15/73 samples have a wide range of VR_{oeqv} from 0.53 to 1.44%, which are measured on the 'net structure' semifusinite (Fig. 3a, 3b) and the wide value range could be attributed to irregular anisotropy.

3.2. Organic geochemistry

TOC and T_{max} data are summarized in Table 2. The results suggest that Baltic shales contain immature samples (Djupvik-2, Core601, and Hällekis-1), early mature samples (Ottenby-2, DBH15/73), and over-mature samples (Porsgrunn, Röverakulan, Klinta, Bjärsjölagård, Gislövhammar, and S.Sandby). It should be noted that the T_{max} values of over-mature samples, e.g., samples from Porsgrunn, are invalid and are not shown in Table 2. T_{max} of these overmature samples is from instrument artifacts since invalid low S2 signal in highly mature source rock (Peters, 1986; Peters and Cassa, 1994; Song et al., 2022; Xiao et al., 2022).

The composite depth profiles of TOC, S2, HI, Inert carbon, T_{max}, and U content of Ottenby-2 samples and DBH15/73 samples are shown in Figs. 6 and 7. These two wells are selected for detailed depth profile analysis since their stratigraphical variation.

In Ottenby-2, the TOC value range from 6.9 to 15.3 wt% in the Miaolingian and Furongian and show an increasing trend stratigraphically. However, it decreases from 12.43 to 7.33 wt% stratigraphically in Tremadocian (Fig. 6a). The oil potential data distribution has a similar trend, with S2 increases from 24.25 to 50.49 mg HC/g stratigraphically in the Furongian while decreases from 53.89 to 29.67 mg HC/g stratigraphically in Tremadocian (Fig. 6b). HI averages around 370 mg HC/g TOC in the Furongian, however, increases to average 430 mg HC/g TOC in the Tremadocian (Fig. 6c). Correspondingly, there is a sudden decrease in the inert carbon content of Tremadocian samples than Furongian samples (Fig. 6d). T_{max} is around 428 °C in Miaolingian while decrease from 430 °C to 420 °C in Furongian and increase gradually stratigraphically in Tremadocian. Besides, there is a typical 'mirror effect' between the depth profile of T_{max} and U (Fig. 8e, 8f).

In DBH15/73, the TOC values gradually increase from averagely 5 wt% in the lower part of Miaolingian section to averagely 8 wt% in the upper part of the Miaolingian section to an average of 15.64 wt% in the Furongian samples (Fig. 7a). The oil potentials are averagely 16.70 mg HC/g in the lower part of Miaolingian samples, averagely 35.2 mg HC/g in the upper part of Miaolingian samples, while averagely 20 mg HC/g in the Furongian samples (Fig. 7b). HI value shows a gradual decreasing trend stratigraphically, with averagely 373 mg HC/g TOC in the lower Miaolingian samples, to 360 mg HC/g

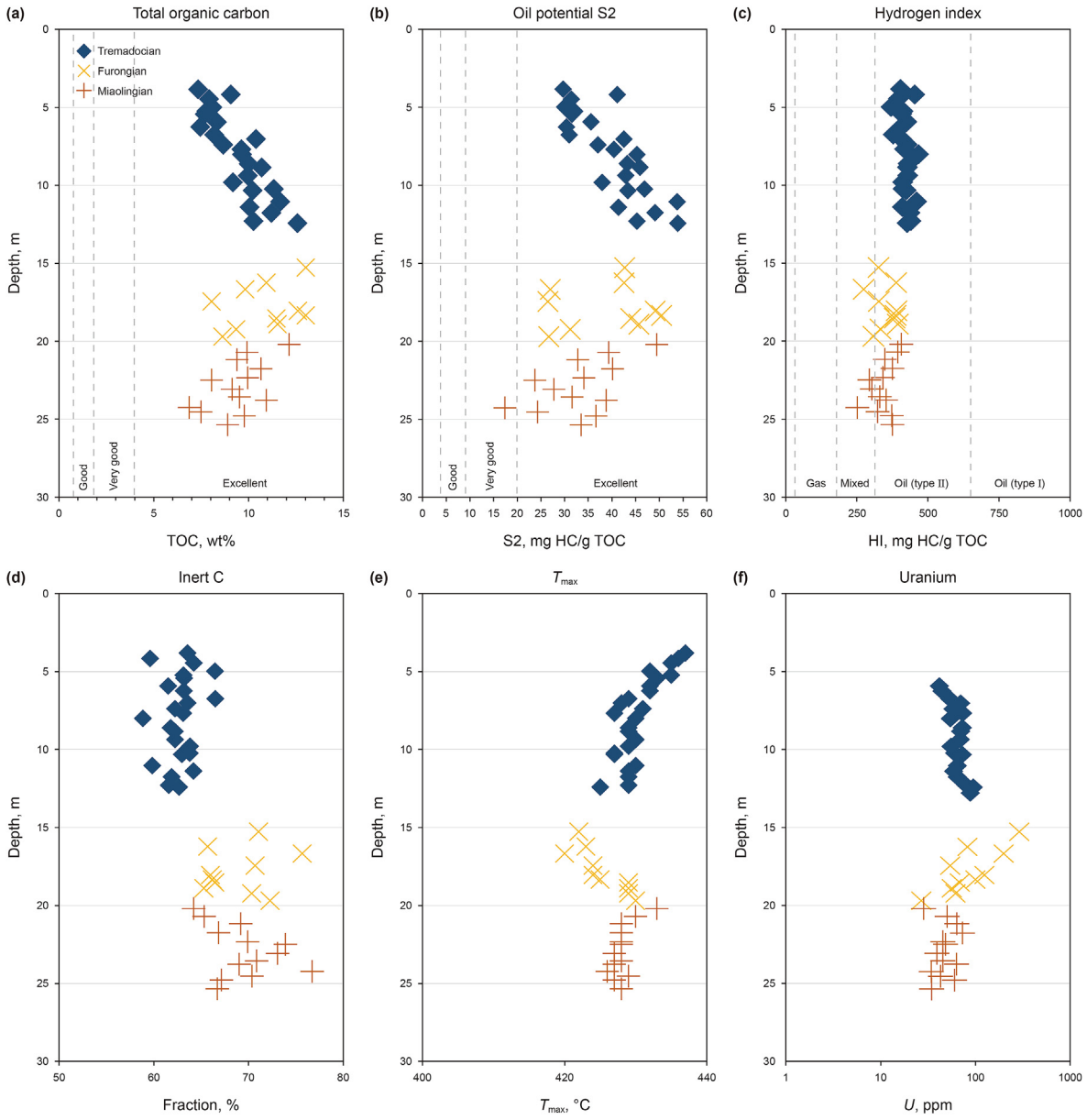

Fig. 6. The Miaolingian-Tremadocian depth profiles of total organic carbon (TOC, wt.%), S2 (mg HC/g), hydrogen index (HI, mg HC/g TOC), inert organic carbon (residual carbon or non-generative organic carbon; wt.%), T_{max} (°C), and uranium (U, ppm) for the Ottenby-2 well.

TOC in the upper Miaolingian samples, to 180 mg HC/g TOC in the Furongian samples (Fig. 7c). The inert carbon content has an increasing trend stratigraphically from 64% in the lower Miaolingian to 70% in the upper Miaolingian to 86% in the Furongian (Fig. 7d). T_{max} decreases from 433 °C to 403 °C stratigraphically (Fig. 7e). The U content distribution also has a 'reverse effect' to T_{max} profile, in the range of 4–422 ppm (Fig. 7f).

4. Discussion

4.1. Sedimentary environment

The TOC and oil potential profile of Ottenby-2 samples (Fig. 6a, 6b) suggest that there is a gradual increase of the enrichment of organic matter during Furongian, followed by a gradual decrease in Tremadocian. The abrupt increase in HI and decrease in inert carbon from Furongian to Tremadocian (Fig. 5c) suggest a predominant OM composition alteration. Such alteration could also be found in organofacies (S2–TOC) plots (Fig. 9), in which the Furongian plots and Tremadocian plots have parallel distribution patterns and regression lines, however, there is a decrease in the X-axis intercept. This suggests that HI increase in Tremadocian is mostly attributed to lower initial dead carbon content (wt%) than Furongian in Ottenby-2. The stable HI values indicate a limited maturation effect, hence the variation in T_{max} profile is probably attributed to U content variation (Fig. 6e and 6f), and the fluctuation distribution in the Furongian could be attributed to the overlap influence of thermal intrusion. Such reverse controlling effect of U content on T_{max} is reported as 'T_{max} suppression' in other works (Dahl et al., 1988; Yang and Horsfield, 2020).

In the data profile of DBH15/73, TOC increase stratigraphically (Fig. 7a). Oil potential and HI profiles suggest that there was an OM degradation in Furongian, which could probably be attributed to the high U content (Fig. 7f) and the local thermal intrusion

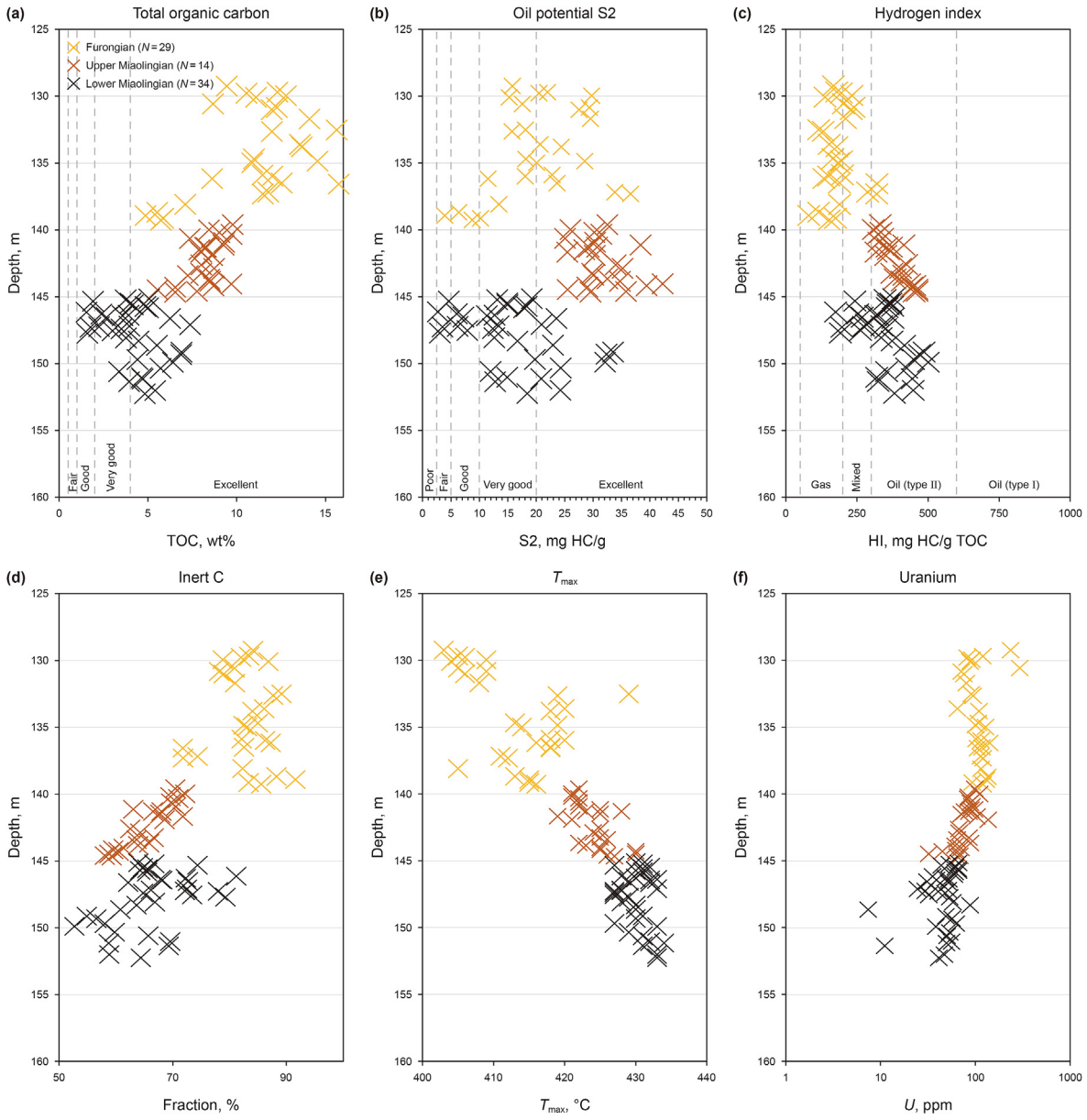

Fig. 7. The Miaolingian-Tremadocian depth profiles of total organic carbon (TOC, wt.%), S1 (mg HC/g), S2 (mg HC/g), hydrogen index (HI, mg HC/g TOC), inert organic carbon (residual carbon or non-generative organic carbon; wt.%), T_{max} (°C), and uranium (U, ppm) for the DBH15/73.

(Buchardt and Lewan, 1990a). This is in accordance with the high inert carbon content in the Furongian (Fig. 7d), which is also shown in the organofacies (S2–TOC) plots with higher inert carbon in the Furongian samples (Fig. 10).

The HI versus T_{max} plot (Fig. 8a) of all the Baltic samples shows that Djupvik-2, Core601, and Hällekis-1 are distributed in the immature phase. While Ottenby-2 and DBH15/73 are partly on the oil zone threshold, suggesting marginal mature. However, it is interesting to find that almost all of the samples have T_{max} lower than 430 °C although the highest VR_{oeqv} of DBH15/73 samples is as high as 1.39% and the average VR_{oeqv} is 0.93%. Few works have reported the T_{max} of samples affected by abnormal maturation from intrusion. However, considering the high uranium content of the Furongian section in DBH15/73 samples, the low T_{max} of these samples could also be partly attributed to T_{max} suppression resulting from uranium enrichment (Dahl et al., 1988; Yang and Horsfield, 2020).

4.2. Organic matter characteristics

Liptinite and their degraded products are the predominant OM fraction in immature Cambrian samples in Baltic shales (Hällekis-1and Miaolingian of DBH15/73). While, the zooclasts fraction, especially graptolite, becomes the major fraction of the OM in Ordovician shales (Djupvik-2, Core601, and the Ordovician section of Ottenby-2). The semifusinite-like macerals identified in the Furongian DBH15/73 samples (Fig. 3a, 3b) are probably derived from quickly matured algal mat. The 'surrounding structure' of the semifusinite-like net around the grain suggests a 'contemporaneous deformation structure' after sedimentation (Fig. 3b). Hence, this *in-situ* structure probably reveals a quick abnormal maturation process, rather than late-oil solid bitumen, a secondary organic matter generated after expulsion and migration. As semifusinite-like are only developed in the Furongian DBH15/73 samples, which corresponds to the wide reflectance value range, it probably

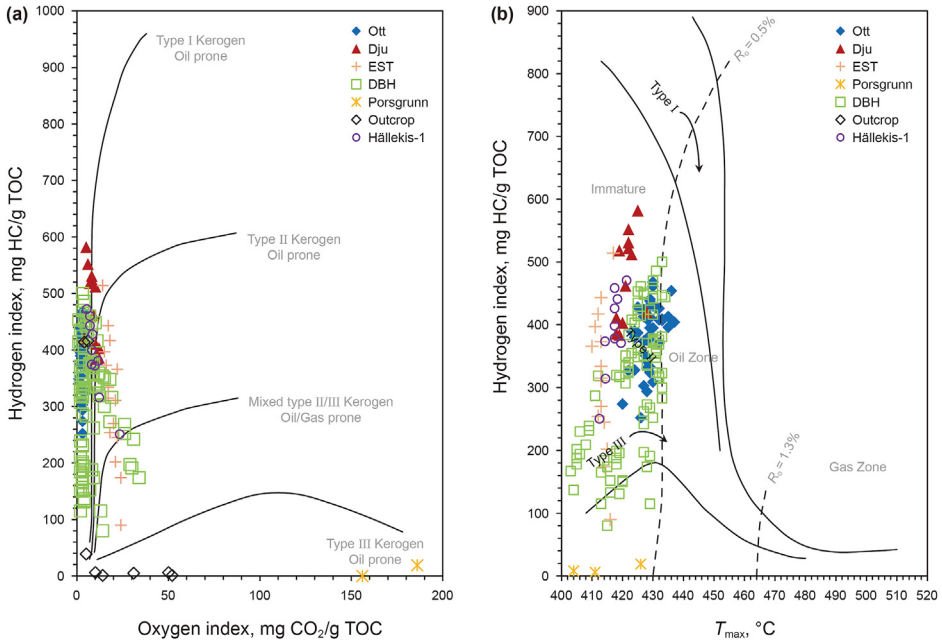

Fig. 8. The Hydrogen Index (HI) vs. T_{max} (left) and pseudo van Krevelen plots of Hydrogen Index (HI) vs. Oxygen Index (OI) (right) of Djupvik-2, Core601, Hällekis-1, Ottenby-2, DBH15/73, Porsgrunn, and outcrops samples from Baltic basin. These suggest diverse kerogen types based on Rock-Eval data.

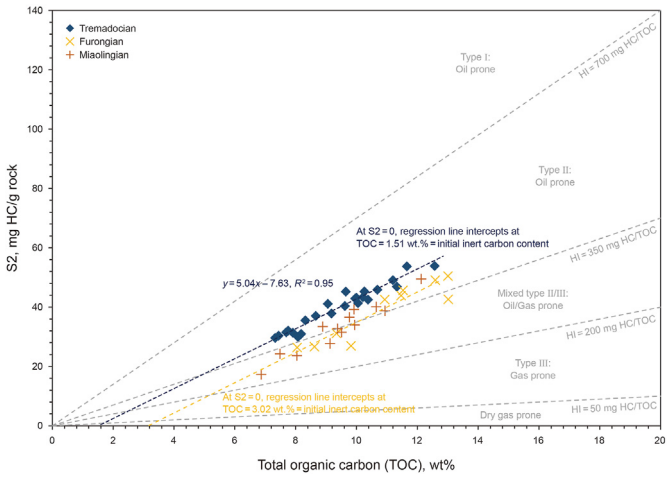

Fig. 9. The organofacies plots of S2 (mg HC/g) vs. TOC (TOC, wt.%) of the upper Cambrian-Lower Ordovician samples from Ottenby-2. The intercept between regression line and *x*-axis indicates the initial inert carbon content according to Cornford (1998) and Cornford et al. (1998).

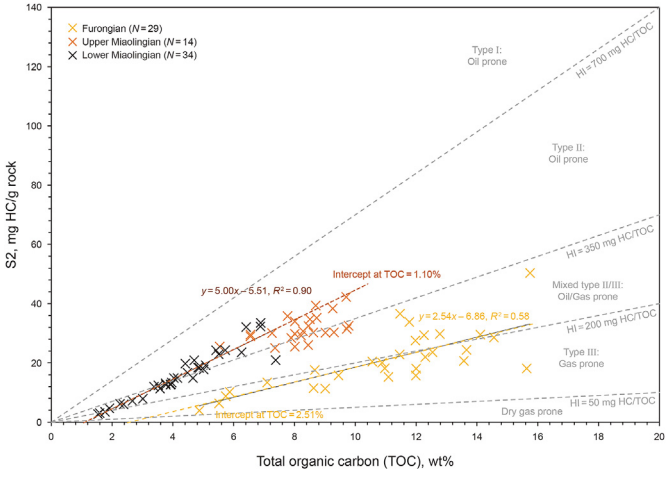

Fig. 10. The organofacies plots of S2 (mg HC/g) vs. TOC (TOC, wt.%) of the lower Cambrian-upper Cambrian samples from DBH15/73. The intercept between regression line and *x*-axis indicates the initial inert carbon content according to Cornford (1998) and Cornford et al. (1998).

indicates a thermal intrusion effect. This is in agreement with a previous report about the local thermal maturation of the kerogen to semi-anthracitic grades resulting from the intrusion of Permo-Carboniferous dolerite dikes in south Sweden (Buchardt et al., 1986).

The maceral observation results of this work, apart from the Furongian DBH15/73 samples, are consistent with previous works. It is also reported that the organic composition of the Scandinavian Alum shale is mainly algal-derived liptinite macerals (fluorescing AOM, lamalginite, telaginite and liptoderinite), graptolite, vitrinite-like particles, and solid bitumen (Petersen et al., 2013; Sanei et al., 2014). The fluorescent organic-clay mixture of natural macerals in Ottenby-2 samples has VR_{oeqv} from 0.61 to 0.74% (mean 0.68%).

4.3. Hydrocarbon generation potential

The pseudo van Krevelen plots (Fig. 8b) of all the Baltic samples could be classified into two groups. One group plotted along the Y-axis, suggesting extremely low OI values. These groups are all Cambrian samples. Such hydrogen-rich characteristics are in accordance with the organic petrology observation of predominantly marine algal-related OM composition in the Cambrian samples. However, samples in other groups are relatively widely distributed and are ranging from type II–oil prone organic matter to type II/III–oil/gas prone organic matter (Fig. 11). Therefore, the distinction between the immature samples suggests that organic matter composition change from Cambrian to Ordovician, which could partly be explained by the kerogen type change from

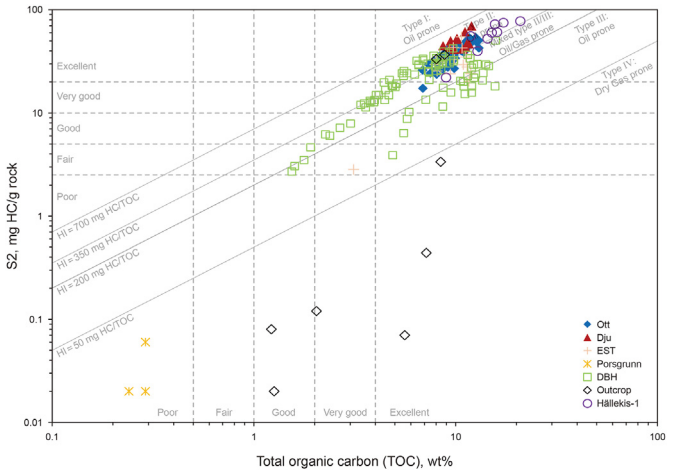

Fig. 11. The S2 vs. TOC plots of Djupvik-2, Core601, Hällekis-1, Ottenby-2, DBH15/73, Porsgrunn, and outcrop samples from Baltic basin. The well samples from Djupvik-2, Core601, Hällekis-1, Ottenby-2, DBH15/73 distribute in type II to type III regions, while Porsgrunn and outcrop samples distribute in type IV region.

autochthonous refractory organic carbon dilution of zooclast particles (Zheng et al., 2021b).

4.4. Hydrocarbon generation model and organofacies

At present time, the measured HI does not reflect the kerogen type due to the thermal maturity and hydrocarbon conversion and expulsion from the initial kerogen (Jones, 1987). Therefore, determining the initial *HI* (HI_o) is an important challenge for the mature and overmature source rocks, and reflects the original organofacies (Jarvie et al., 2007; Chen and Jiang, 2015). The *HI* restoration formula with Rock-Eval data (Chen and Jiang, 2015) was applied in this work to HI_o as below:

$$HI = HI_o\left[1 - \exp\left\{-\left(\frac{T_{max}}{\beta}\right)^{\theta}\right\}\right] + c \quad (1)$$

where HI_o, β, and θ are unknown parameters specific to kerogen kinetics, of which HI_o characterizes the hydrocarbon generation history, β represents the temperature threshold for massive hydrocarbon generation, while θ represents the oil window, and c is a constant reflecting the measured *HI* error in high T_{max} (Chen and Jiang, 2015). By fitting Eq. (1) through the plotting data of T_{max} vs. *HI*, the most suitable model could be estimated, which has the optimal HI_o, β, θ, and c to reflect the general hydrocarbon generation process covering the data set.

As constraint data played a significant role in determining the fitting regression line, uranium-rich Furongian samples (100–300 ppm) were removed from the data set Fig. 12. Because their T_{max} and *HI* values had been greatly affected by dike intrusion in the bulk geochemistry and were not suitable to be applied as immature lower Paleozoic benchmarks. Besides, some mature Alum shale samples from published data (Kosakowski et al., 2016) were applied in this model. This mathematical model was calculated with Matlab with 'non-linear least squares' as the fitting option. The fitting result and coefficient of 95% confidence limits are HI_o: 400 mg HC/g TOC (369.5 mg HC/g TOC, 430.5 mg HC/g TOC), β: 441.9 °C (436.2 °C, 447.5 °C), θ: 29.48 (−48.51, −10.46) and '*c*' equals to 0. The best-fitting line and prediction intervals of 90%, 60%, and 30% are also shown in Fig. 12. The *HI* values of immature samples sitting in a relatively wide range from 320 to 520 mg HC/g TOC

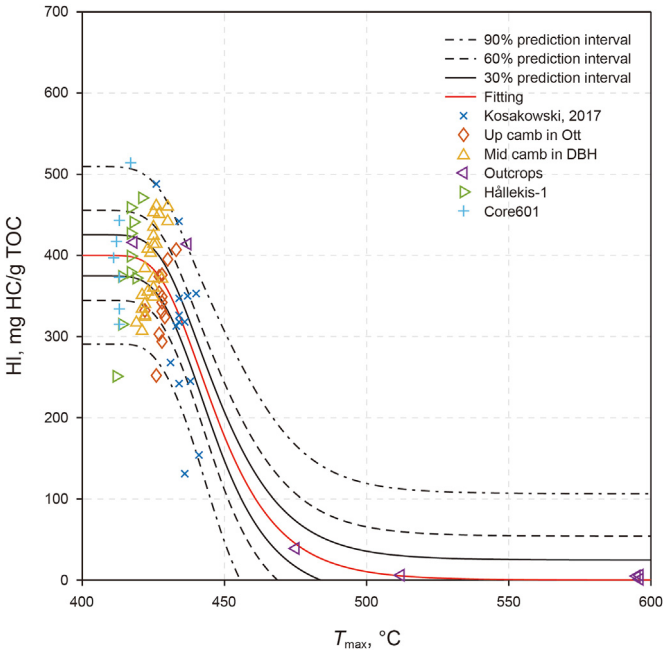

Fig. 12. *HI* versus T_{max} and fitted non-linear regression model based on Eq (1), the fitting line is calculated with Matlab with 'non-linear least squares' as the fitting option and coefficient of 95% confidence limits are HI_o: 420 mg HC/g TOC.

could be attributed to organic matter composition heterogeneous. Generally, these values are very close to the P90 (340 mg HC/g TOC) to P50 (475 mg HC/g TOC) value range of the HI_o calculated from a worldwide marine shale database (Jarvie, 2012).

This *HI* range of immature shales and the $HI_{ocalculated}$ of 400 mg HC/g TOC from the mature and over mature samples suggest that the sample set could be categorized mainly into organofacies B and minor into organofacies BC based on the organic facies classification (Jones, 1987). Both organic facies B and BC suggest anoxic-dysoxic facies, according to Jone's organic facies concept. Jones (1987) proposed that organic facies BC represents sediments with a relatively high phytoclast input, e.g., terrestrial and reworked OM, while organic facies B has relatively low phytoclast input (Jones, 1987). However, in this work, the organic facies BC classified from lower HI_o could be attributed to abundant zooclastic fragments. It is also reported that the enrichment of non-generative organic carbon-rich graptolite cuticle leading to autochthonous refractory organic carbon dilution, causing marine type II kerogen to shift towards type II+III kerogen, and measured HI underestimation (Zheng et al., 2021b).

5. Conclusions

This study investigates the organic matter composition and thermal maturity distribution of the Cambrian-Ordovician shale samples from the Baltic Basin in Scandinavia. These samples have a wide maturity range from immature to overmature. The organic petrology results show that Cambrian shales are mainly composed of alginite, AOM, bituminite and solid bitumen, while, there is an increase of the zooclast constituents in the Ordovician source rocks. As the maturity increases, post-oil solid bitumen becomes the dominant OM constituent. HI_o calculation model: $HI = HI_o$ [1−exp {−(T_{max}/β)^θ }]+c is simulated based on pyrolysis data and fitted according to the least-square fitting method, with restored HI_o of 400 mg HC/g TOC (369.5 mg HC/g TOC to 430.5 mg HC/g TOC as 95% coefficient confidence bounds). The restored HI_o and present *HI* of

immature samples show that all the samples represent organofacies B, which is the most widespread type of organic facies in most of the world's source rock and indicates a marine anoxia and transgressive sea with the shallow water column.

Acknowledgments

The authors would like to thank the great supports from the State Key Laboratory of Shale Oil and Gas Enrichment, Sinopec for providing precious data and samples. Dr. Runhai Feng (Copenhagen University) is thanked for assisting and guiding in modeling with Matlab. We acknowledge the financial and technical support of the Lower Paleozoic Consortium including the State Key Laboratory of Petroleum Resources and Prospecting in China University of Petroleum-Beijing (CUP), Chinese Scholarship Council (CSC), and Geological Survey of Denmark and Greenland (GEUS).

References

Buchardt, B., Lewan, M.D., 1990. Reflectance of vitrinite-like macerals as a thermal maturity index for cambrian-ordovician Alum shale, southern Scandinavia. AAPG (Am. Assoc. Pet. Geol.) Bull. 74, 394–406. https://doi.org/10.1306/0C9B230D-1710-11D7-8645000102C1865D.

Buchardt, B., Clausen, J., Thomsen, E., 1986. Carbon isotope composition of lower Paleozoic kerogen: effects of maturation, 1986 Org. Geochem. 10 (1–3), 127–134. https://doi.org/10.1016/0146-6380(86)90016-1.

Cai, Q.S., Hu, M.Y., Zhang, B.M., et al., 2022. Source of silica and its implications for organic matter enrichment in the Upper Ordovician-Lower Silurian black shale in western Hubei Province, China: insights from geochemical and petrological analysis. Petrol. Sci. 19 (1), 74–90. https://doi.org/10.1016/j.petsci.2021.10.012.

Chen, Z., Jiang, C., 2015. A data driven model for studying kerogen kinetics with application examples from Canadian sedimentary basins. Mar. Petrol. Geol. 67, 795–803. https://doi.org/10.1016/j.marpetgeo.2015.07.004.

Cornford, C., 1998. Source rocks and hydrocarbons of the north sea. Petroleum geology of the North Sea: Basic concepts and recent advances 376–462. https://doi.org/10.1002/9781444313413.ch11.

Cornford, C., Gardner, P., Burgess, C., 1998. Geochemical truths in large data sets. I: geochemical screening data. Org. Geochem. 29 (1–3), 519–530. https://doi.org/10.1016/S0146-6380(98)00189-2.

Dahl, J., Hallberg, R., Kaplan, I.R., 1988. The effects of radioactive decay of uranium on elemental and isotopic ratios of Alum Shale kerogen. Appl. Geochem. 3 (6), 583–589. https://doi.org/10.1016/0883-2927(88)90090-X.

Ding, X., He, W., Liu, H., et al., 2022. Organic matter accumulation in lacustrine shale of the permian jimsar sag, junggar basin, NW China. Petrol. Sci. https://doi.org/10.1016/j.petsci.2022.11.004.

Erlström, M., Thomas, S.A., Deeks, N., Sivhed, U., 1997. Structure and tectonic evolution of the Tornquist Zone and adjacent sedimentary basins in Scania and the southern Baltic Sea area. Tectonophysics 271 (3–4), 191–215. https://doi.org/10.1016/s0040-1951(96)00247-8.

Espitalié, J., Madec, M., Tissot, B., Mennig, J.J., Leplat, P., 1977. May. Source rock characterization method for petroleum exploration. In: *Offshore Technology Conference*. OnePetro.

Hackley, P.C., Valentine, B.J., Hatcherian, J.J., 2018. On the petrographic distinction of bituminite from solid bitumen in immature to early mature source rocks. Int. J. Coal Geol. 196, 232–245. https://doi.org/10.1016/j.coal.2018.06.004.

Horsfield, B., Bharati, S., Larter, S.R., Leistner, F., Littke, R., Schenk, H.J., Dypvik, H., 1992. On the atyptical Petroleum-generating characteristics of Alginite in the Cambrian Alum Shale. In: Schidlowski, M., Golubic, S., Kimberley, M., McKirdy, D., Trudinger, P.A. (Eds.), Early Organic Evolution. Springer, Berlin Heidelberg, pp. 257–266.

Hu, T., Pang, X., Jiang, S., et al., 2018. Oil content evaluation of lacustrine organic-rich shale with strong heterogeneity: a case study of the Middle Permian Lucaogou Formation in Jimusaer Sag, Junggar Basin, NW China. Fuel 221, 196–205. https://doi.org/10.1016/j.fuel.2018.02.082.

Hu, T., Pang, X., Jiang, F., et al., 2021. Movable oil content evaluation of lacustrine organic-rich shales: methods and a novel quantitative evaluation model. Earth Sci. Rev. 214, 103545. https://doi.org/10.1016/j.earscirev.2021.103545.

ICCP, 2001. The new inertinite classification (ICCP System 1994). Fuel 80, 459–471. https://doi.org/10.1016/S0016-2361(00)00102-2.

Jacob, H., 1989. Classification, structure, genesis and practical importance of natural solid bitumen (migrabitumen). Int. J. Coal Geol. 11 (1), 65–79. https://doi.org/10.1016/0166-5162(89)90113-4.

Jarvie, D.M., 2012. Shale resource systems for oil and gas: Part 1—shale-gas resource systems. AAPG (Am. Assoc. Pet. Geol.) Bull. 97, 69–87. https://doi.org/10.1306/13321446M973489.

Jarvie, D.M., Hill, R.J., Ruble, T.E., et al., 2007. Unconventional shale-gas systems: the Mississippian Barnett Shale of north-central Texas as one model for thermogenic shale-gas assessment. AAPG (Am. Assoc. Pet. Geol.) Bull. 91 (4), 475–499. https://doi.org/10.1306/12190606068.

Jones, R.W., 1987. Organic facies. In: Brooks, J., Welte, D. (Eds.), Advances in Petroleum Geochemistry. Academic Press, New York, pp. 1–90.

Kosakowski, P., Kotarba, M.J., Piestrzyński, A., et al., 2016. Petroleum source rock evaluation of the Alum and dictyonema shales (upper cambrian–lower ordovician) in the Baltic Basin and podlasie depression (eastern Poland). Int. J. Earth Sci. 106 (2), 743–761. https://doi.org/10.1007/s00531-016-1328-x.

Liu, X.B., Liu, G.D., Jiang, W.Y., et al., 2022. Organic geochemistry and petrology of source rocks from the banqiao sag, bohai bay basin, China: implications for petroleum exploration. Petrol. Sci. 19 (4), 1505–1515. https://doi.org/10.1016/j.petsci.2022.07.002.

Luo, Q., Hao, J., Skovsted, C.B., et al., 2017. The organic petrology of graptolites and maturity assessment of the Wufeng–Longmaxi Formations from Chongqing, China: insights from reflectance cross-plot analysis. Int. J. Coal Geol. 183, 161–173. https://doi.org/10.1016/j.coal.2017.09.006.

Luo, Q., Fariborz, G., Zhong, N., Wang, Y., Qiu, N., Skovsted, C.B., Suchý, V., Schovsbo, N.H., Morga, R., Xu, Y., Hao, J., 2020. Graptolites as fossil geothermometers and source material of hydrocarbons: an overview of four decades of progress. Earth Sci. Rev. 200, 103000.

Nielsen, A.T., Schovsbo, N., 2006. Cambrian to basal Ordovician lithostratigraphy in southern Scandinavia. Bull. Geol. Soc. Den. 53, 47–92. ISSN 0011–6297. www.2dgf.dk/publikationer/bulletin.

Nielsen, A.T., Høyberget, M., Ahlberg, P., 2020. The furongian (upper cambrian) Alum shale of Scandinavia: revision of zonation. Lethaia 53 (4), 462–485. https://doi.org/10.1111/let.12370.

Pan, J., Ge, T., Liu, W., et al., 2021. Organic matter provenance and accumulation of transitional facies coal and mudstone in Yangquan, China: insights from petrology and geochemistry. J. Nat. Gas Sci. Eng. 94, 104076. https://doi.org/10.1016/j.jngse.2021.104076.

Pang, P., Han, H., Tan, X., et al., 2022. Organic matter pores in the chang 7 lacustrine shales from the Ordos Basin and its effect on reflectance measurement. Petrol. Sci. https://doi.org/10.1016/j.petsci.2022.08.031.

Peters, K.E., 1986. Guidelines for evaluating petroleum source rock using programmed pyrolysis. AAPG (Am. Assoc. Pet. Geol.) Bull. 70, 318–329. https://doi.org/10.1306/94885688-1704-11D7-8645000102C1865D.

Peters, K.E., Cassa, M., 1994. Applied Source Rock Geochemistry. AAPG Memoir, p. 60.

Petersen, H.I., Schovsbo, N.H., Nielsen, A.T., 2013. Reflectance measurements of zooclasts and solid bitumen in Lower Paleozoic shales, southern Scandinavia: correlation to vitrinite reflectance. Int. J. Coal Geol. 114 (30), 1–18. https://doi.org/10.1016/j.coal.2013.03.013.

Pickel, W., Kus, J., Flores, D., et al., 2017. Classification of liptinite – ICCP system 1994. Int. J. Coal Geol. 169, 40–61. https://doi.org/10.1016/j.coal.2016.11.004.

Sanei, H., 2020. Genesis of solid bitumen. Scientific Report 10 (1), 1–10. https://doi.org/10.1038/s41598-020-72692-2.

Sanei, H., Petersen, H.I., Schovsbo, N.H., et al., 2014. Petrographic and geochemical composition of kerogen in the Furongian (U. Cambrian) Alum Shale, central Sweden: Reflections on the petroleum generation potential. Int. J. Coal Geol. 132, 158–169. https://doi.org/10.1016/j.coal.2014.08.010.

Schovsbo, N.H., Nielsen, A.T., Erlström, M., 2016. Middle–upper ordovician and silurian stratigraphy and basin development in southernmost Scandinavia. Bull. Geol. Soc. Den. 35, 39–42. https://doi.org/10.34194/geusb.v35.4907.

Schovsbo, N.H., Nielsen, A.T., Harstad, A.O., et al., 2018. Stratigraphy and geochemical composition of the cambrian Alum Shale Formation in the Porsgrunn core, skien-Langesund district, southern Norway. Bull. Geol. Soc. Den. 66 (1). https://doi.org/10.37570/bgsd-2018-66-01.

Schulz, H.M., Yang, S., Schovsbo, N.H., et al., 2021. The furongian to lower ordovician Alum Shale Formation in conventional and unconventional petroleum systems in the Baltic Basin – a review. Earth Sci. Rev. 218, 103674. https://doi.org/10.1016/j.earscirev.2021.103674.

Song, D.F., Wang, T.G., Li, P., et al., 2022. Petrology and organic geochemistry of the baishaping and damaidi devonian cutinitic liptobioliths, west of the Kangdian uplift, China. Petrol. Sci. 19 (5), 1978–1992. https://doi.org/10.1016/j.petsci.2022.07.012.

Thorslund, P., 1968. The ordovician-silurian boundary below Gotland. Geol. Foren. Stockh. Forh. 90 (3), 443–451. https://doi.org/10.1080/11035896809448415.

Tissot, B.P., Welte, D.H., 1984. Petroleum formation and occurrence. Springer, pp. 153–165.

Wang, Y., Chang, X., Liu, Z., et al., 2022. Occurrence state and oil content evaluation of Permian Fengcheng Formation in the Hashan area as constrained by NMR and multistage Rock-Eval. Petrol. Sci. https://doi.org/10.1016/j.petsci.2022.11.019.

Xiao, X.M., Wilkins, R.W.T., Dehan, L., et al., 2000. Investigation of thermal maturity of lower Palaeozoic hydrocarbon source rocks by means of vitrinite-like maceral reflectance — a Tarim Basin case study. Org. Geochem. 31 (10), 1041–1052. https://doi.org/10.1016/S0146-6380(00)00061-9.

Xiao, H., Li, M.J., Wang, T.G., et al., 2022. Discovery of a new proterozoic paleoreservoir and its oil source in the jianchang sag, Yanliao faulted-depression zone, north China. Petrol. Sci. 19 (5), 1927–1938. https://doi.org/10.1016/j.petsci.2022.08.025.

Xu, Q., Liu, B., Song, X., et al., 2022. Hydrocarbon generation and organic matter enrichment of limestone in a lacustrine mixed sedimentary environment: a case study of the Jurassic Da'anzhai member in the central Sichuan Basin, SW China. Petrol. Sci. https://doi.org/10.1016/j.petsci.2022.10.002.

Yang, S., Horsfield, B., 2020. Critical review of the uncertainty of Tmax in revealing the thermal maturity of organic matter in sedimentary rocks. Int. J. Coal Geol.

225, 103500. https://doi.org/10.1016/j.coal.2020.103500.
Zheng, X., Schovsbo, N.H., Bian, L., et al., 2021a. Alteration of organic macerals by uranium irradiation in lower Paleozoic marine shales. Int. J. Coal Geol. 239, 103713. https://doi.org/10.1016/j.coal.2021.103713.
Yang, S., Schulz, H.M., Horsfield, B., Schovsbo, N.H., Noah, M., Panova, E., Rothe, H., Hahne, K., 2018. On the changing petroleum generation properties of Alum Shale over geological time caused by uranium irradiation. Geochem. Cosmochim. Acta 229, 20–35. https://doi.org/10.1016/j.gca.2018.02.049.
Zheng, X., Sanei, H., Schovsbo, N.H., et al., 2021b. Role of zooclasts in the kerogen type and hydrocarbon potential of the lower Paleozoic Alum Shale. Int. J. Coal Geol. 248, 103865. https://doi.org/10.1016/j.coal.2021.103865.
Zheng, X., Schovsbo, N.H., Luo, Q., et al., 2022. Graptolite reflectance anomaly. Int. J. Coal Geol. 261, 104072. https://doi.org/10.1016/j.coal.2022.104072.
Zhu, C., Jiang, F., Zhang, P., et al., 2022. Effect of petroleum chemical fraction and residual oil content in saline lacustrine organic-rich shale: a case study from the Paleogene Dongpu depression of North China. Petrol. Sci. https://doi.org/10.1016/j.petsci.2022.09.013.